Realization of a magnonic analog adder with frequency-division multiplexing

Cite as: AIP Advances 13, 015115 (2023); doi: 10.1063/5.0120826
Submitted: 15 August 2022 • Accepted: 15 December 2022 •
Published Online: 12 January 2023

Frank Schulz,[1,a] Felix Groß,[1] Johannes Förster,[1] Sina Mayr,[2,3] Markus Weigand,[4] Eberhard Goering,[1] Joachim Gräfe,[1] Gisela Schütz,[1] and Sebastian Wintz[1]

AFFILIATIONS

[1] Max-Planck-Institut für Intelligente Systeme, 70569 Stuttgart, Germany
[2] Paul-Scherrer-Institut, 5232 Villigen, Switzerland
[3] Laboratory for Mesoscopic Systems, Department of Materials, ETH Zurich, 8093 Zurich, Switzerland
[4] Helmholtz-Zentrum Berlin für Materialien und Energie, 12489 Berlin, Germany

[a] **Author to whom correspondence should be addressed:** fschulz@is.mpg.de

ABSTRACT

Being able to accurately control the interaction of spin waves is a crucial challenge for magnonics in order to offer an alternative wave-based computing scheme for certain technological applications. Especially in neural networks and neuromorphic computing, wave-based approaches can offer significant advantages over traditional CMOS-based binary computing schemes with regard to performance and power consumption. In this work, we demonstrate precise modulation of phase- and amplitude-sensitive interference of coherent spin waves in a yttrium–iron–garnet based magnonic analog adder device, while also showing the feasibility of frequency-division multiplexing. Using time-resolved scanning transmission x-ray microscopy, the interference was directly observed, giving an important proof of concept for this kind of analog computing device and its underlying working principle. This constitutes a step toward wave-based analog computing using magnons as an information carrier.

I. INTRODUCTION

While a computer based on binary logic is in principle able to solve the problems that arise in machine learning, it may not be the most efficient one at doing so.[1–4] Instead, recent approaches have shifted their focus toward alternative computing schemes, which are more suitable for the kinds of calculations that need to be performed in neural networks.[5,6] This includes, but is not limited to, reservoir-, stochastic-, and neuromorphic computing.[7–10] Machine learning and neuromorphic computing can be implemented in terms of ordinary binary logic; however, in order to reduce both power consumption and the number of components needed, it can be beneficial to depart from the binary approach. One avenue is analog computing, which is taking advantage of the, in the classical limit, continuous nature of physical quantities in order to perform information processing and calculations. Historically, this has already been done more than two thousand years ago using mechanical systems to predict astronomical events and more recently using electrical circuits[6,11] or even optical methods.[12]

Another framework in which analog computing can be realized is found in the research field of magnonics.[13–17] Magnons, which are bosonic quasi-particles corresponding to the collective precession of magnetic moments, have recently been studied as a possible information carrier. They can propagate in magnetic materials, both insulators and conductors, in the form of coherent spin waves, and due to the lack of charge transport, energy losses caused by Joule heating are minimized. It also opens the possibility of wave based computing, where both the amplitude information and phase information of the spin wave are used for data processing, and interference effects can be exploited.[18–22] This can also be combined with the field of spintronics, where both spin-polarized currents and pure spin-currents are used for precise control of magnetic systems on the micrometer scale and below.[23–26] These approaches offer a vast number of possibilities for the realization of information processing devices, while also giving insight into the underlying physics.[27–32]

Much of the work performed on magnon based information processing has focused on binary logic gates and circuits, but it

is also possible to use magnonic systems for analog computing. Recently, a concept for an analog adder for all-magnonic neurons was proposed,[33] but so far, it has not been experimentally realized. A nanoscale spin-wave interferometer utilizing exchange spin waves has been realized; however, the experimental technique did not allow for resolution in k-space and phase.[20]

In this work, we present the experimental realization of an Yttrium–Iron–Garnet (YIG) based magnonic analog adder with frequency-division multiplexing, where the continuous nature of the spin-wave amplitude is used for performing non-binary addition operations. By utilizing time-resolved scanning transmission x-ray microscopy (TR-STXM), we directly image spin-wave interference of arbitrary amplitudes and relative phase with both spatial and temporal resolution.

First, the interference conditions are characterized by varying the relative phase between the spin waves emitted by two microstrips, showing complete destructive interference, constructive interference, and several states in between. By systematically varying the amplitudes of the excitation signals, the functionality of the device as an analog adder is confirmed, representing an experimental proof of concept for a magnon based analog computing device. The device is also shown to allow for frequency-division multiplexing by superimposing multiple signals with different frequencies at each input and disentangling the resulting spin-wave pattern by means of fast Fourier transform (FFT) analysis.

While readout has been realized using x-ray optical methods in this work, others have shown that readout of spin-wave intensity is also possible electrically,[34] demonstrating, in principle, compatibility with electrical circuits.

II. EXPERIMENTAL DETAILS

Commercially available ferrimagnetic YIG films with a thickness of 100 nm (Innovent Jena) were used as a basis for the devices. The films are grown on a Gadolinium–Gallium–Garnet (GGG) substrate using liquid phase epitaxy. YIG films of the same supplier have been shown to possess a crystalline structure with extremely low Gilbert damping α on the order of $1 \cdot 10^{-4}$ and spin-wave propagation lengths beyond 30 μm.[35,36]

Micro-patterning was performed using electron-beam lithography on a Raith Eline at an acceleration voltage of 20 kV, utilizing a conductive polymer (ESpacer) to reduce charging effects in the insulating substrate. With this, two 500 nm wide microstrips with a 2 μm gap, as well as wider leads and bonding pads to establish electrical contact, were defined on top of the YIG film. A stack of Cr(8 nm)/Cu(180 nm)/Cr(8 nm) was then deposited using a Leybold UNIVEX thermal evaporation chamber, and the lift-off procedure was performed with n-methyl-2-pyrrolidon at 70 °C. This structure allowed for the excitation of spin waves by means of coupling of the microstrips' Oersted fields to the magnetic moments of the YIG film. For that, radio-frequency (RF) signals with frequencies between 2.57 and 3.07 GHz were transmitted through the microstrips.

The sample was thinned mechanically from the GGG side, first uniformly down to 120 μm thickness with a very fine abrasive paper and then locally down to 20 μm using a dimple grinder. In the last step, the focused ion beam (FIB) of a dual beam Nova 600 NanoLab by FEI was used to create an x-ray transparent window of ~$30 \times 30\ \mu m^2$ size with a thickness of about 200 nm.

Spin-wave dynamics are recorded as a series of snapshots in time ("movies") using time-resolved scanning transmission x-ray microscopy (TR-STXM) at the MAXYMUS end station at the BESSY II electron storage ring operated by the *Helmholtz-Zentrum Berlin für Materialien und Energie*. For that, an asynchronous pump-probe scheme with a double lock-in technique is used, allowing us to measure the samples' magnetization component along the x-ray beam axis with both spatial and temporal resolution.[37] Exemplary movies of the time-resolved magnetization dynamics can be found in the supplementary material. All measurements were performed at room temperature and at the L_3 edge of Fe, where the x-ray magnetic circular dichroism (XMCD) effect gives rise to magnetic contrast due to the different absorption depending on the relative alignment of the x-ray photon angular momentum and the sample magnetization.[38]

Further post-processing using an FFT algorithm is carried out in order to separate individual oscillation frequencies,[39] allowing us to study the samples' capability of frequency-division multiplexing.

For the study of spin-wave interference, the two microstrips could be excited independently with different amplitudes and an arbitrary phase shift between the two excitations using an arbitrary waveform generator with two independent output channels.[40] To this end, the generator outputs are connected via coaxial cables to the coplanar signal lines of a printed circuit board that carries the sample. These lines are in turn connected to one of the two ends of each microstrip on the sample. The output side of each microstrip is eventually terminated via 50 Ω to ground. While the ground of the generator is connected to the ground of the board, the sample itself does not have coplanar signal lines and is not connected to ground. Despite this missing ground, we did not observe any significant direct or capacitive microwave crosstalk between the two microstrip antennas, owing to the electrically insulating properties of YIG.

III. RESULTS AND DISCUSSION

A sketch of the sample can be seen in Fig. 1, with the thinned down x-ray transparent window in the center. The microwave signal that is applied to the two microstrips generates a magnetic field around them. This Oersted field can then couple to the magnetic moments in the YIG film, giving rise to magnetic oscillations that travel through the film in the form of spin waves.[41,42] The wavelength of the RF signal in the figure is not to scale; it is several orders of magnitude longer in reality.

An external magnetic field $\mathbf{B}$, which is applied parallel to the microstrips, allows for the excitation of Damon–Eshbach type spin waves, where the wave vector $\mathbf{k}$ is perpendicular to the external field $\mathbf{B}$ and hence the samples' equilibrium magnetization ($\mathbf{M} \perp \mathbf{k}$).[43] In order to excite coherent spin-wave dynamics, the magnetic field has to be of sufficient magnitude to saturate the sample and match the dispersion relation.[44] A three-dimensional rendering of the obtained spin-wave pattern can be seen in the center of Fig. 1; the area marked with dashed lines is additionally displayed in the inset and shows a snapshot of the dynamic out-of-plane magnetization component m_z. It is evident that the excitation of the Damon–Eshbach spin waves is highly asymmetric with respect to the microstrips, which almost

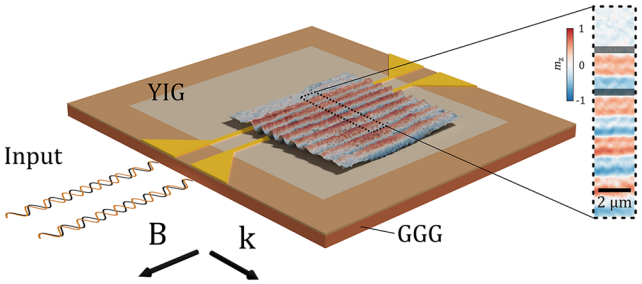

FIG. 1. Schematic of the magnonic analog adder device, with the thinned x-ray transparent window in the center. An RF signal with a frequency of 2.57 GHz (black) and 3.07 GHz (orange) is applied to both microstrips (RF wavelength not to scale). Three-dimensional rendering of the resulting dynamical spin-wave interference pattern with the wave-vector **k**, as imaged by TR-STXM. An external magnetic field of 28 mT was applied in-plane, parallel to the microstrips. The inset shows a magnified view of the area marked with dashed lines, with the color indicating the normalized out-of-plane magnetization m_z and the microstrips marked in gray.

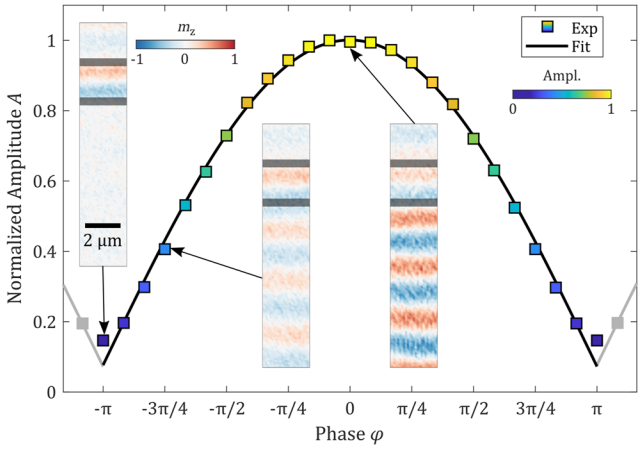

FIG. 2. Normalized amplitude A of the spin-wave interference pattern as a function of relative normalized phase φ, together with the theoretical prediction for two interfering sine-waves. Measurements were performed with an external field of 28 mT and an excitation frequency of 2.72 GHz. The insets show examples of recorded spin-wave patterns, from which the amplitude was obtained, with the color indicating the normalized out-of-plane magnetization m_z.

exclusively emit spin waves in one direction (downward in the inset of Fig. 1). This is a well-known effect originating from the orientation of the Oersted field around the microstrip with respect to the local deflection of magnetic moments in the spin wave.[45] Since the device is operated in the linear regime, the low amplitude spin waves propagating in the opposite direction do not influence interference in the main direction.

All measurements shown here are obtained at input voltages where the signal amplitude of the TR-STXM measurements is proportional to the deflection of the magnetic moments in the YIG film and hence to the local amplitude of the spin waves. In addition, the power was kept low enough to keep the Joule heating low, which would otherwise change the magnetization of the YIG film. A locally reduced magnetization would lead to a change in the wavelength, which would in turn alter the interference conditions. This also means that it is not feasible to study nonlinear effects such as two-magnon scattering while preserving the interference conditions.

For a quantitative analysis, which is crucial for showing the feasibility of a magnon-based analog adder, the amplitude of the spin-wave pattern was obtained by means of a fast Fourier transform analysis. Previous works have shown that this approach yields great improvement in the signal-to-noise ratio since only the oscillations with the desired frequency are included in the output signal, whereas other contributions, such as those coming from electrical crosstalk and other noise, will be filtered out.[37] What is obtained by applying the FFT analysis is a number of frequency slices corresponding to the base frequency and integer multiples thereof. The number of frequency slices is given by the number of frames recorded using the pump-probe scheme. This is especially useful when it comes to frequency-division multiplexing, which will be discussed in the last part of this work and can also be realized in a straightforward way for electronic readout. The spin-wave amplitude will be given throughout the text in terms of normalized amplitude, where the values ±1 correspond to a spin-wave deflection angle of ±1.7°. The deflection angle was obtained by following the procedure described in Ref. 37, justifying the small-angle approximation.

In order to operate an interference-based analog adder, the interference conditions have to be characterized, which was done by altering the phase shift between the inputs at the two microstrips with respect to each other. Figure 2 shows the normalized amplitude of the spin-wave interference pattern as a function of the relative normalized phase between the two inputs φ for an excitation frequency of 2.72 GHz at an externally applied field of 28 mT. The amplitude was obtained by averaging the amplitude of the Fourier transform corresponding to the base frequency in the area adjacent to the second microstrip. The insets show the recorded spin-wave patterns corresponding to the data points in the graph, for which a wavelength of 2.6 µm is observed. Owing to the experimental technique used, both amplitude and phase information were obtained in one measurement, revealing the underlying mechanism of spin-wave interference in a clear manner. The individual spin waves excited at the two microstrips interfere, depending on their relative phase, either constructively or destructively, resulting in the observed interference pattern. A closer look on the inset at $\varphi = 0$ reveals that backward volume spin waves are also excited in the YIG layer, recognizable by the faint diagonal stripes. However, due to their relatively small amplitude, they do not affect the functionality of the adder device. These backward volume type spin waves presumably arise from small inhomogeneities in the microstrips or the film itself and have been observed in several other TR-STXM experiments simultaneously with Damon–Eshbach waves in different materials.[39,46]

The Damon–Eshbach type spin waves here are expected to be of sinusoidal form, and we are operating the analog adder device in the linear regime, where interfering spin waves can be described by their linear superposition. The amplitude of the resulting spin wave, traveling along the x-direction, at one moment in time, can therefore be described by

$$\sin(kx) + \sin(kx + \varphi) = 2\cos\left(\frac{\varphi}{2}\right) \cdot \sin\left(kx + \frac{\varphi}{2}\right). \quad (1)$$

The fit function shown in Fig. 2 is of the form $a \cdot \cos(\frac{\varphi}{2}) + b$ to fit the amplitude of the resulting spin wave as a function of relative phase. Different path lengths in the electrical setup, as well as the fact that the spin waves from the upper microstrip have to traverse the distance between the microstrips, introduce a phase shift that needs to be compensated for. This was carried out experimentally by continuously varying the phase shift in order to minimize the spin-wave amplitude (complete destructive interference) and defining this to be $\varphi = \pi$. All phases are then given in terms of the relative normalized phase with respect to this value. In addition, the excitation amplitudes were chosen so that complete destructive interference would occur, accounting for different resistances and also the attenuation of the spin waves from the top microstrip on their way to the lower microstrip. Once the phase for destructive interference was determined, spin-wave movies were recorded for different phases in steps of $\pi/4$, showing everything from complete destructive interference ($\varphi = \pm\pi$) to complete constructive interference ($\varphi = 0$), with their amplitude following the behavior established by Eq. (1). Only the data point at complete destructive interference shows a slight deviation from the expected trend, as some signal still remains. However, this is an artifact originating from the FFT analysis for signals with a poor signal-to-noise ratio, which can also be seen in the corresponding inset. The snapshots also reveal that the spin-wave amplitude between the two microstrips is independent of φ due to the asymmetric excitation of spin waves in the Damon–Eshbach geometry. Between the microstrips, we only observe the spin wave originating from the top. When it reaches the lower microstrip, it interferes with the spin wave that is excited there. Owing to the insulating properties of YIG, crosstalk between the microstrips is reduced compared to a conductive magnetic thin film. For electrical readout, a third microstrip can be placed at a distance from the first two microstrips.[34]

Knowing the phase that is needed for constructive interference, it is now possible to verify the functionality of the device as a magnonic analog adder. So far, the spin waves at the two microstrips were excited with the same amplitude. Now, in order to show the addition capabilities of the device, the phase is set to $\varphi = 0$, leading to constructive interference. The input signal amplitudes U_1 and U_2 of the two microstrip excitation signals are then varied while recording the spin-wave interference pattern.

Figure 3(a) shows the normalized spin-wave amplitude landscape as a function of the two signal amplitudes for an excitation frequency of 3.07 GHz and an external field of 28 mT. As a first step, the procedure for determining the phase in which constructive interference occurs was repeated for this new frequency. The amplitude of the excitation signals U_1 and U_2 is given in terms of the voltage amplitude of the signal that was sent to the microstrips, as measured by an oscilloscope using a directional coupler right before the sample. The continuous landscape was obtained by linear interpolation between the data points.

This was also used to add equiamplitude lines at the mean value of the data points that should yield the same result for a working adder device, namely, data points, for which the sum of U_1 and U_2 is equal.

It can be seen that the individual data points align almost perfectly with the equiamplitude lines, illustrating the commutative property $(a + b = b + a)$, as well as the general functionality $(1 + 5 = 2 + 4 = 3 + 3)$, of the addition operation in the analog adder

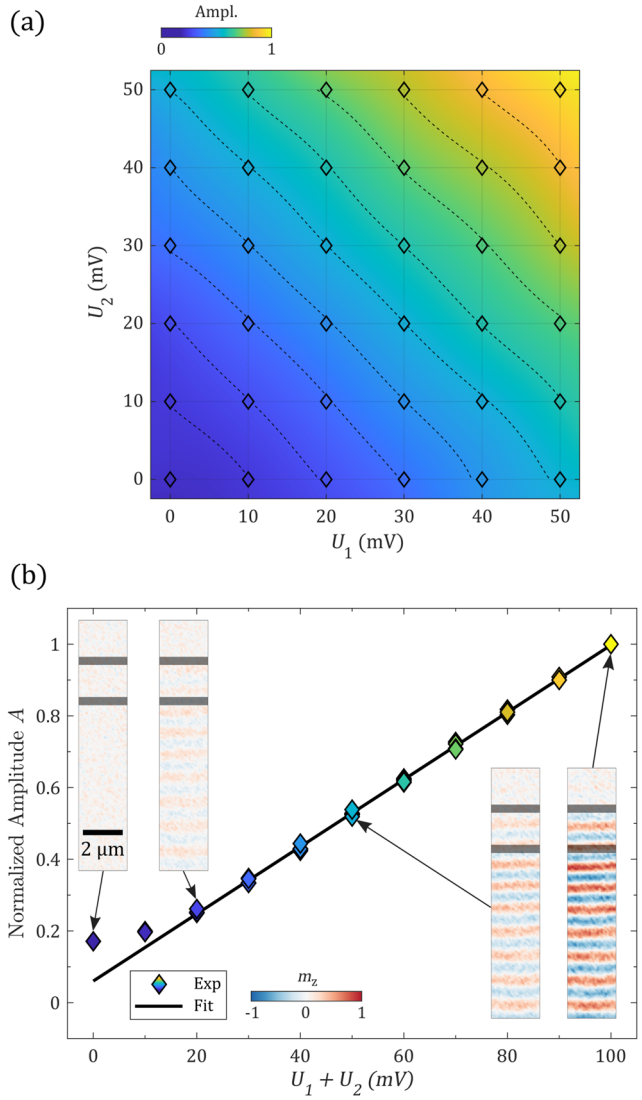

FIG. 3. Constructive interference of two spin waves excited at 3.07 GHz with an external field of 28 mT. (a) Landscape of the normalized amplitude A of the spin-wave interference pattern as a function of the excitation amplitude at the two microstrips U_1 and U_2. Experimental data points are marked by diamonds, and equiamplitude lines are marked by dashes; the color gradient from linear interpolation is a guide to the naked eye. (b) Normalized amplitude as a function of the sum of the two excitation signals $U_1 + U_2$. Experimental data (colored diamonds) with a linear fit (line). The insets show examples of the recorded spin-wave movies from which the amplitude was obtained, with the color indicating the normalized out-of-plane magnetization m_z.

device. Again, each data point in the landscape corresponds to a spin-wave movie, where the amplitude was obtained by averaging the FFT amplitude corresponding to the base excitation frequency in the area below the second microstrip.

The device is operating in the linear regime, which means that the normalized amplitude is proportional to the sum of the two excitation signals $U_1 + U_2$, as can be seen in Fig. 3(b). It also means

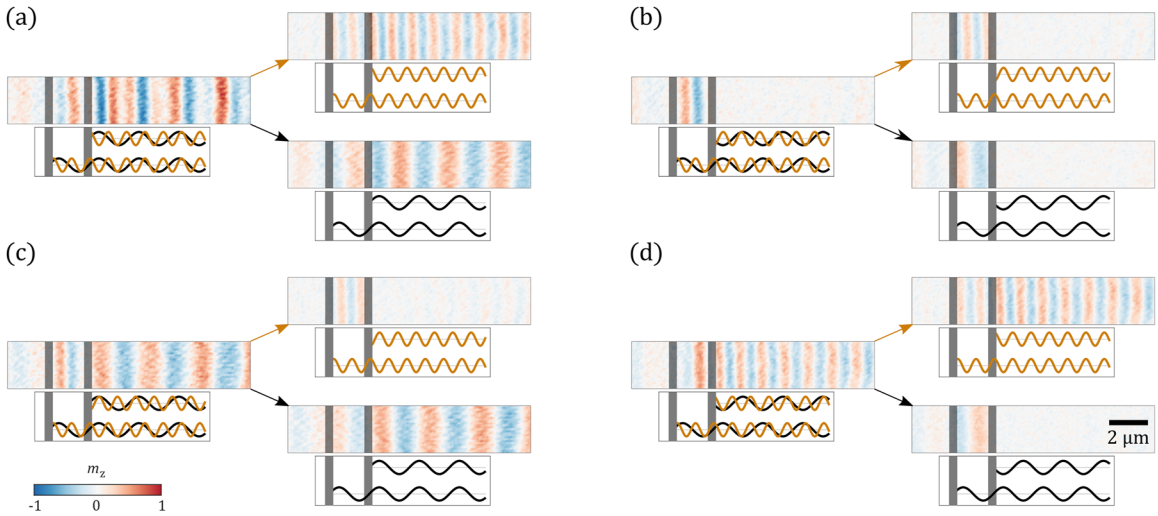

FIG. 4. Overview of the frequency-division multiplexing capabilities of the magnonic analog adder device. Each microstrip is excited with a signal consisting of a 2.72 GHz (black) and a 3.07 GHz (orange) component. From the recorded TR-STXM movies, the two components could be retrieved using a fast Fourier transformation (orange and black arrows). This is done for (a) full constructive interference, (b) full destructive interference, (c) constructive 2.72 GHz and destructive 3.07 GHz, and (d) destructive 2.72 GHz and constructive 3.07 GHz. The color indicates the normalized out-of-plane magnetization m_z.

that doubling the input will result in twice the spin-wave signal, an important property of an analog adder. Similar to the case of complete destructive interference in Fig. 2, it is once again visible that for very low amplitudes, the FFT evaluation yields a value >0; however, the linear behavior is restored at higher amplitudes, as shown by the linear fit for the range between 20 and 100 mV. For each value on the x-axis, all data points corresponding to that sum are plotted on top of each other. It is found that they align within an error margin of 2%, which can be further reduced using an electrical setup, which should be the ultimate goal in order to enable compatibility with other electrical circuits.

The insets in Fig. 3(b) again show TR-STXM measurements over a 2.5×12.5 µm^2 area corresponding to the individual data points, measured at an external field of 28 mT. The steady increase in the spin-wave amplitude is clearly visible, and it is also evident that the wavelength has changed compared to the measurements at 2.72 GHz seen in Fig. 2. The wavelength is observed to be 1.1 µm, and the reduction compared to the previous measurements is in accordance with the dispersion relation of a magnetic thin film with in-plane magnetization.[44]

In order to demonstrate the feasibility of frequency-division multiplexing, the two microstrips were each excited with a superposition of two frequencies, namely, 2.72 and 3.07 GHz. In the linear regime, this excitation mode will result in the superposition of two spin waves propagating from each of the two microstrips. This was done for different phase shifts between the two components to cover all four possible cases of constructive and destructive interference for the two frequencies.

These four combinations are shown in Figs. 4(a)–4(d), with the spin-wave patterns presented alongside a sketch that shows the individual components. On the left side, the recorded spin-wave patterns are shown, and by applying the FFT evaluation procedure, it is possible to break down this signal into its frequency components (indicated by the arrows), namely, 2.72 GHz (black arrow, bottom) and 3.07 GHz (orange arrow, top). A version with the complete spin-wave movie can be found in the supplementary material. In Fig. 4(a), both frequency components interfere constructively, resulting in a rather complicated spin-wave pattern, which, when disentangled, yields the fundamental waves. Figure 4(b) shows the case where both components interfere destructively, and, apart from the area between the two microstrips, there's no spin-wave signal. The sketch of the spin waves illustrates the phase shift of π between the waves coming from the left and the right microstrip, resulting in the destructive interference for both components. In Fig. 4(c), the short wavelength 3.07 GHz component interferes destructively due to the phase shift of π, and the long wavelength 2.72 GHz component interferes constructively. Finally, in Fig. 4(d), the opposite case is shown.

It is important to keep in mind that in all four cases, a signal with both frequency components is used to excite the microstrips; it is only via destructive interference that one of the components is not visible in the resulting spin-wave pattern. This nicely demonstrates that it is possible to control the interference of each component individually, while also being able to distinguish between the two frequency components, which is also possible in an electrical setup as long as the measurement is phase sensitive or has some other means of demultiplexing. The device, therefore, is demonstrated to be capable of frequency-division multiplexing in the linear regime, a crucial feature when it comes to computational efficiency and performance.

IV. CONCLUSIONS

The experimental realization of a magnonic analog adder based on spin-wave interference was demonstrated. In an insulating, magnetic YIG thin film, spin waves were excited by means of an RF

signal that was transmitted through two conductive microstrips. The spin-wave interference was quantitatively analyzed as a function of the relative phase between the two input signals using TR-STXM. Different interference patterns, ranging from complete constructive to complete destructive interference, were observed, and their amplitudes were compared to theoretical predictions. Addition was demonstrated by quantitative analysis of the amplitude of the spin-wave pattern in the case of constructive interference as a function of excitation signal amplitude, showing excellent linear behavior, as well as the commutative property. By varying the relative phase by π, the presented device is easily reconfigurable to perform analog subtraction. The chosen measurement method also allowed for direct validation of the frequency-division multiplexing capabilities of the device, with the possibility to break down the measured interference pattern into its frequency components.

Overall, this shows that the concept of a magnon-based analog adder is indeed feasible, representing an important step toward analog computing using spin waves.

SUPPLEMENTARY MATERIAL

The supplementary material contains animated movies of the experimental data. This includes a 3D rendition of a single spin wave propagating through the YIG film, an animated version of Fig. 4, and videos of two spin waves interfering constructively and destructively at 2.72 and 3.07 GHz, respectively.

ACKNOWLEDGMENTS

We want to thank Barbara Baum and Annette Zechmeister for cutting the samples, Ulrike Eigenthaler and Thomas Meisner for thinning them, and Marion Hagel for vacuum deposition of the microstrips. We thank the Helmholtz-Zentrum Berlin for the allocation of synchrotron radiation beamtime. S.M. acknowledges funding from the Swiss National Science Foundation, under Grant Agreement No. 172517.

AUTHOR DECLARATIONS

Conflict of Interest

The authors have no conflicts to disclose.

Author Contributions

Frank Schulz: Conceptualization (equal); Data curation (equal); Formal analysis (equal); Investigation (equal); Methodology (equal); Writing – original draft (equal). **Felix Groß**: Formal analysis (equal); Methodology (supporting); Writing – review & editing (supporting). **Johannes Förster**: Formal analysis (equal); Investigation (equal). **Sina Mayr**: Data curation (equal); Investigation (equal); Writing – review & editing (equal). **Markus Weigand**: Methodology (equal); Resources (equal). **Eberhard Goering**: Funding acquisition (equal); Writing – review & editing (equal). **Joachim Gräfe**: Conceptualization (supporting); Methodology (equal); Project administration (supporting); Supervision (supporting). **Gisela Schütz**: Funding acquisition (equal); Project administration (equal); Resources (equal). **Sebastian Wintz**: Conceptualization (equal); Data curation (equal); Formal analysis (equal); Methodology (equal); Project administration (equal); Supervision (equal); Writing – original draft (equal); Writing – review & editing (equal).

DATA AVAILABILITY

The data that support the findings of this study are available from the corresponding author upon reasonable request.

REFERENCES

[1] V. Sze, Y.-H. Chen, J. Emer, A. Suleiman, and Z. Zhang, "Hardware for machine learning: Challenges and opportunities," in *2017 IEEE Custom Integrated Circuits Conference (CICC)* (IEEE, 2017), pp. 1–8.
[2] K. Berggren, Q. Xia, K. K. Likharev, D. B. Strukov, H. Jiang, T. Mikolajick, D. Querlioz, M. Salinga, J. R. Erickson, S. Pi *et al.*, "Roadmap on emerging hardware and technology for machine learning," Nanotechnology **32**, 012002 (2020).
[3] M. Hu, Y. Chen, J. J. Yang, Y. Wang, and H. H. Li, "A compact memristor-based dynamic synapse for spiking neural networks," IEEE Trans. Comput.-Aided Des. Integr. Circuits Syst. **36**, 1353–1366 (2016).
[4] Q. Wan, M. T. Sharbati, J. R. Erickson, Y. Du, and F. Xiong, "Emerging artificial synaptic devices for neuromorphic computing," Adv. Mater. Technol. **4**, 1900037 (2019).
[5] F. Rosenblatt, "The perceptron: A probabilistic model for information storage and organization in the brain," Psychol. Rev. **65**, 386–408 (1958).
[6] H. P. Graf, "Analog electronic neural networks," in *European Solid-State Circuits Conference September 1992* (IEEE, 1992), pp. 57–60.
[7] G. Tanaka, T. Yamane, J. B. Héroux, R. Nakane, N. Kanazawa, S. Takeda, H. Numata, D. Nakano, and A. Hirose, "Recent advances in physical reservoir computing: A review," Neural Networks **115**, 100–123 (2019); arXiv:1808.04962.
[8] B. R. Gaines, "Stochastic computing," in *Proceedings of the April 18–20, 1967, Spring Joint Computer Conference* Association for Computing Machinery, (New York, 1967), pp. 149–156.
[9] A. Alaghi and J. P. Hayes, "Survey of stochastic computing," Trans. Embedded Comput. Syst. **12**, 1–19 (2013).
[10] G. W. Burr, R. M. Shelby, A. Sebastian, S. Kim, S. Kim, S. Sidler, K. Virwani, M. Ishii, P. Narayanan, A. Fumarola, L. L. Sanches, I. Boybat, M. Le Gallo, K. Moon, J. Woo, H. Hwang, and Y. Leblebici, "Neuromorphic computing using non-volatile memory," Adv. Phys. X **2**, 89–124 (2017).
[11] I. B. Pyne, "Linear programming on an electronic analogue computer," Trans. Am. Inst. Electr. Eng., Part 1 **75**, 139–143 (1956).
[12] D. R. Solli and B. Jalali, "Analog optical computing," Nat. Photonics **9**, 704–706 (2015).
[13] A. V. Chumak, V. I. Vasyuchka, A. A. Serga, and B. Hillebrands, "Magnon spintronics," Nat. Phys. **11**, 453–461 (2015).
[14] V. V. Kruglyak, S. O. Demokritov, and D. Grundler, "Magnonics," J. Phys. D: Appl. Phys. **43**, 264001 (2010).
[15] A. Chumak, P. Kabos, M. Wu, C. Abert, C. Adelmann, A. Adeyeye, J. Åkerman, F. Aliev, A. Anane, A. Awad *et al.*, "Advances in magnetics roadmap on spin-wave computing," IEEE Trans. Magn. **58**, 0800172 (2022).
[16] A. Barman, G. Gubbiotti, S. Ladak, A. O. Adeyeye, M. Krawczyk, J. Gräfe, C. Adelmann, S. Cotofana, A. Naeemi, V. I. Vasyuchka *et al.*, "The 2021 magnonics roadmap," J. Phys.: Condens. Matter **33**, 413001 (2021).
[17] B. Lenk, H. Ulrichs, F. Garbs, and M. Münzenberg, "The building blocks of magnonics," Phys. Rep. **507**, 107–136 (2011); arXiv:1101.0479.
[18] W. Zhu, H. Qin, L. Flajšman, T. Taniyama, and S. Van Dijken, "Zero-field routing of spin waves in a multiferroic heterostructure," Appl. Phys. Lett. **120**, 112407 (2022).
[19] O. Rousseau, B. Rana, R. Anami, M. Yamada, K. Miura, S. Ogawa, and Y. Otani, "Realization of a micrometre-scale spin-wave interferometer," Sci. Rep. **5**, 9873 (2015).

[20]J. Chen, H. Wang, T. Hula, C. Liu, S. Liu, T. Liu, H. Jia, Q. Song, C. Guo, Y. Zhang, J. Zhang, X. Han, D. Yu, M. Wu, H. Schultheiss, and H. Yu, "Reconfigurable spin-wave interferometer at the nanoscale," Nano Lett. **21**, 6237–6244 (2021).
[21]M. Balinskiy, D. Gutierrez, H. Chiang, Y. Filimonov, A. Kozhevnikov, and A. Khitun, "Spin wave interference in YIG cross junction," AIP Adv. **7**, 056633 (2017).
[22]Á. Papp, W. Porod, and G. Csaba, "Nanoscale neural network using non-linear spin-wave interference," Nat. Commun. **12**, 6422 (2021); arXiv:2012.04594.
[23]J. E. Hirsch, "Spin hall effect," Phys. Rev. Lett. **83**, 1834 (1999).
[24]S. D. Bader and S. S. P. Parkin, "Spintronics," Annu. Rev. Condens. Matter Phys. **1**, 71–88 (2010).
[25]I. Žutić, J. Fabian, and S. D. Sarma, "Spintronics: Fundamentals and applications," Rev. Mod. Phys. **76**, 323 (2004).
[26]V. S. Pribiag, I. N. Krivorotov, G. D. Fuchs, P. M. Braganca, O. Ozatay, J. C. Sankey, D. C. Ralph, and R. A. Buhrman, "Magnetic vortex oscillator driven by dc spin-polarized current," Nat. Phys. **3**, 498–503 (2007).
[27]G. Dieterle, J. Förster, H. Stoll, A. S. Semisalova, S. Finizio, A. Gangwar, M. Weigand, M. Noske, M. Fähnle, I. Bykova *et al.*, "Coherent excitation of heterosymmetric spin waves with ultrashort wavelengths," Phys. Rev. Lett. **122**, 117202 (2019).
[28]M. Baumgartner, K. Garello, J. Mendil, C. O. Avci, E. Grimaldi, C. Murer, J. Feng, M. Gabureac, C. Stamm, Y. Acremann *et al.*, "Spatially and time-resolved magnetization dynamics driven by spin–orbit torques," Nat. Nanotechnol. **12**, 980–986 (2017).
[29]S. Wintz, V. Tiberkevich, M. Weigand, J. Raabe, J. Lindner, A. Erbe, A. Slavin, and J. Fassbender, "Magnetic vortex cores as tunable spin-wave emitters," Nat. Nanotechnol. **11**, 948–953 (2016).
[30]A. V. Chumak, A. A. Serga, and B. Hillebrands, "Magnon transistor for all-magnon data processing," Nat. Commun. **5**, 4700 (2014).
[31]P. Wadley, B. Howells, J. Železný, C. Andrews, V. Hills, R. P. Campion, V. Novák, K. Olejník, F. Maccherozzi, S. S. Dhesi, S. Y. Martin, T. Wagner, J. Wunderlich, F. Freimuth, Y. Mokrousov, J. Kuneš, J. S. Chauhan, M. J. Grzybowski, A. W. Rushforth, K. Edmonds, B. L. Gallagher, and T. Jungwirth, "Spintronics: Electrical switching of an antiferromagnet," Science **351**, 587–590 (2016).
[32]M. Madami, S. Bonetti, G. Consolo, S. Tacchi, G. Carlotti, G. Gubbiotti, F. B. Mancoff, M. A. Yar, and J. Åkerman, "Direct observation of a propagating spin wave induced by spin-transfer torque," Nat. Nanotechnol. **6**, 635–638 (2011).
[33]T. Brächer and P. Pirro, "An analog magnon adder for all-magnonic neurons," J. Appl. Phys. **124**, 152119 (2018); arXiv:1806.01389.
[34]G. Talmelli, T. Devolder, N. Träger, J. Förster, S. Wintz, M. Weigand, H. Stoll, M. Heyns, G. Schütz, I. P. Radu, J. Gräfe, F. Ciubotaru, and C. Adelmann, "Reconfigurable submicrometer spin-wave majority gate with electrical transducers," Sci. Adv. **6**, eabb4042 (2020).
[35]C. Dubs, O. Surzhenko, R. Linke, A. Danilewsky, U. Brückner, and J. Dellith, "Sub-micrometer yttrium iron garnet LPE films with low ferromagnetic resonance losses," J. Phys. D: Appl. Phys. **50**, 204005 (2017).
[36]J. Förster, J. Gräfe, J. Bailey, S. Finizio, N. Träger, F. Gross, S. Mayr, H. Stoll, C. Dubs, O. Surzhenko *et al.*, "Direct observation of coherent magnons with sub-optical wavelengths in a single-crystalline ferrimagnetic insulator," Phys. Rev. B **100**, 214416 (2019).
[37]F. Groß, N. Träger, J. Förster, M. Weigand, G. Schütz, and J. Gräfe, "Nanoscale detection of spin wave deflection angles in permalloy," Appl. Phys. Lett. **114**, 012406 (2019).
[38]G. Schütz, W. Wagner, W. Wilhelm, P. Kienle, R. Zeller, R. Frahm, and G. Materlik, "Absorption of circularly polarized x rays in iron," Phys. Rev. Lett. **58**, 737 (1987).
[39]N. Träger, F. Groß, J. Förster, K. Baumgaertl, H. Stoll, M. Weigand, G. Schütz, D. Grundler, and J. Gräfe, "Single shot acquisition of spatially resolved spin wave dispersion relations using X-ray microscopy," Sci. Rep. **10**, 18146 (2020).
[40]F. Groß, N. Träger, F. Schulz, M. Weigand, T. Dippon, and J. Gräfe, "A high frequency builder software for arbitrary radio frequency signals," Rev. Sci. Instrum. **93**, 034704 (2022).
[41]T. Stückler, C. Liu, T. Liu, H. Yu, F. Heimbach, J. Chen, J. Hu, S. Tu, Y. Zhang, S. Granville *et al.*, "Ultrabroadband spin-wave propagation in $Co_2(Mn_{0.6}Fe_{0.4})$ Si thin films," Phys. Rev. B **96**, 144430 (2017).
[42]F. Ciubotaru, T. Devolder, M. Manfrini, C. Adelmann, and I. P. Radu, "All electrical propagating spin wave spectroscopy with broadband wavevector capability," Appl. Phys. Lett. **109**, 012403 (2016).
[43]R. W. Damon and J. R. Eshbach, "Magnetostatic modes of a ferromagnet slab," J. Phys. Chem. Solids **19**, 308–320 (1961).
[44]B. A. Kalinikos and A. N. Slavin, "Theory of dipole-exchange spin wave spectrum for ferromagnetic films with mixed exchange boundary conditions," J. Phys. C: Solid State Phys. **19**, 7013 (1986).
[45]P. Wessels, A. Vogel, J.-N. Tödt, M. Wieland, G. Meier, and M. Drescher, "Direct observation of isolated Damon-Eshbach and backward volume spin-wave packets in ferromagnetic microstripes," Sci. Rep. **6**, 22117 (2016).
[46]J. Förster, S. Wintz, J. Bailey, S. Finizio, E. Josten, C. Dubs, D. A. Bozhko, H. Stoll, G. Dieterle, N. Träger, J. Raabe, A. N. Slavin, M. Weigand, J. Gräfe, and G. Schütz, "Nanoscale X-ray imaging of spin dynamics in yttrium iron garnet," J. Appl. Phys. **126**, 173909 (2019); arXiv:1903.00498.